J|A|C|S
ARTICLES
Published on Web 02/21/2002

Magnetic Properties of a Homologous Series of Vanadium Jarosite Compounds

Dimitris Papoutsakis, Daniel Grohol, and Daniel G. Nocera*

Contribution from the Department of Chemistry, 6-335, Massachusetts Institute of Technology, 77 Massachusetts Avenue, Cambridge, Massachusetts 02139-4307

Received August 13, 2001

Abstract: Redox-based, hydrothermal synthetic methodologies have enabled the preparation of a new series of stoichiometrically pure jarosites of the formula, $AV_3(OH)_6(SO_4)_2$ with A = Na^+, K^+, Rb^+, Tl^+, and NH_4^+. These jarosites represent the first instance of strong ferromagnetism within a Kagomé layered framework. The exchange interaction, which is invariant to the nature of the A^+ ion ($\Theta_{CW} \approx +53(1)$ K), propagates along the d^2 magnetic sites of the triangular Kagomé lattice through bridging hydroxyl groups. An analysis of the frontier orbitals suggests this superexchange pathway to possess significant π-orbital character. Measurements on a diamagnetic host jarosite doped with magnetically dilute spin carriers, $KGa_{2.96}V_{0.04}(OH)_6(SO_4)_2$, reveal significant single-ion anisotropy for V^{3+} ion residing in the tetragonal crystal field. This anisotropy confines the exchange-coupled moments to lie within the Kagomé layer. Coupling strengths are sufficiently strong to prevent saturation of the magnetization when an external field is applied orthogonal to the Kagomé layer. Antiferromagnetic ordering of neighboring ferromagnetic Kagomé layers becomes dominant at low temperatures, characteristic of metamagnetic behavior for the $AV_3(OH)_6(SO_4)_2$ jarosites. This interlayer exchange coupling decreases monotonically with increasing layer spacing along the series, A = Na^+, K^+, Rb^+, NH_4^+, and Tl^+, and it may be overcome by the application of external field strengths in excess of ~6 kOe.

Introduction

The two-dimensional connection of triangles through shared vertices produces the extended plaquette known as the Kagomé lattice. Unusual magnetic properties including spin frustration[1] may result when unpaired spins are situated at the triangular corners of this lattice type. Despite intense interest in their magnetic ground states,[1−3] the systematic investigation of Kagomé lattices has been precluded by the paucity of Kagomé-based materials. The layered garnet, $SrGa_{12-x}Cr_xO_{19}$ ($SCGO_x$), has been intensively investigated;[4−8] however, interpretation of its magnetic properties is complicated by the presence of an additional triangular (non-Kagomé) lattice interposed between Kagomé layers. Conversely, the mineral jarosite, $KFe_3(OH)_6(SO_4)_2$, is composed solely of Kagomé layers formed by $Fe^{III}_3(\mu\text{-}OH)_3$ triangles. These triangles are capped by sulfate groups positioned alternately up and down about the hexagonal network.[9] The Kagomé layers are separated by K^+ cations, which reside in the interlayer space with the same x,y crystallographic coordinates as the sulfur atoms of the capping tetrahedra. A family of jarosite compounds arises from the substitution of the Fe^{3+} ions with other M^{3+} ions (Cr^{3+}, Al^{3+}, Ga^{3+}, In^{3+}) and the substitution of the K^+ cation by other monovalent (Na^+, Rb^+, Ag^+, Tl^+, NH_4^+, H_3O^+) or divalent ($^1/_2Pb^{2+}$, $^1/_2Hg^{2+}$) cations; two more members of the jarosite family result from the replacement of the sulfate group by either SeO_4^{2-} or CrO_4^{2-}.[9,10] The ability to systematically vary the intra- and interlayer metal ions, interlayer spacing and the dimensions of the intralayer triangles with the tetrahedral capping anion offers jarosites as a unified framework in which to correlate magnetism with the structural and electronic properties of a Kagomé lattice.

Yet magnetism studies of jarosites are hampered by the inability to prepare chemically pure samples. So far, synthetic routes to jarosites have exclusively relied on the precipitation of solids from hydrolyzed acidic solutions of sulfate anions and monovalent and trivalent cations.[11] Under these conditions, the monovalent cations are susceptible to replacement by hydronium ions; occupancy of the M^{3+} lattice sites is typically only 83−94%. Owing to the presence of these site defects, the magnetic behavior of jarosites has historically been sample dependent.[10,12] The imperative to obtain reliable and reproducible magnetic measurements prompted us to develop new hydrothermal

(1) Ramirez, A. P. *Annu. Rev. Mater. Sci.* **1994**, *24*, 453−480.
(2) Shender, E. F.; Holdsworth, P. C. W. In *Fluctuations and Order*, Millonas, M., Ed.; Springer-Verlag: Berlin, 1996; p 259.
(3) Solin, S. A. *Annu. Rev. Mater. Sci.* **1997**, *27*, 89−115.
(4) Lee, S.-H.; Broholm, C.; Aeppli, G.; Perring, T. G.; Hessen, B.; Taylor, A. *Phys. Rev. Lett.* **1996**, *76*, 4424−4427.
(5) Broholm, C.; Aeppli, G.; Espinosa, G. P.; Cooper, A. S. *Phys. Rev. Lett.* **1990**, *65*, 3173−3176.
(6) Ramirez, A. P.; Espinosa, G. P.; Cooper, A. S. *Phys. Rev. Lett.* **1990**, *64*, 2070−2073.
(7) Keren, A.; Mendels, P.; Horvatic, M.; Ferrrer, F.; Uemura, Y. J.; Mekata, M.; Asano, T. *Phys. Rev. B* **1998**, *57*, 10745−10749.
(8) Keren, A.; Uemura, Y. J.; Luke, G.; Mendels, P.; Mekata, M.; Asano, T. *Phys. Rev. Lett.* **2000**, *84*, 3450−3453.
(9) Jambor, J. L. *Can. Mineral.* **1999**, *37*, 1323−1341.
(10) Wills, A. S.; Harrison, A. *J. Chem. Soc., Faraday Trans.* **1996**, *92*, 2161−2166.
(11) Dutrizac, J. E. *Metall. Trans. B* **1983**, *14*, 531−539.
(12) Wills, A. S.; Harrison, A.; Ritter, C.; Smith, R. I. *Phys. Rev. B* **2000**, *61*, 6156−6169.

10.1021/ja016833m CCC: $22.00

methods in which the magnetic M^{3+} ions are generated by an oxidation−reduction reaction.[13] These redox-based methods, which yield stoichiometrically pure and crystalline materials, are general to metal ion substitution, enabling us to explore how the magnetism of the Kagomé lattice of jarosites varies with the d-electron count of the M^{3+} ion.

Jarosites typically exhibit antiferromagnetic coupling within the Kagomé layer. The strength of the exchange interaction is largest ($\Theta_{CW} = -800$ K) for the parent $Fe^{3+}(d^5)$ jarosite.[12−17] Replacement of the Fe^{3+} centers with $Cr^{3+}(d^3)$ also affords an antiferromagnetically ordered material but with a significantly reduced Weiss constant ($\Theta_{CW} = -67$ K).[18,19] The d-count of the jarosites has been expanded to early transition metals with our recent preparation of the V^{3+} jarosite compound, $NaV_3(OH)_6(SO_4)_2$.[20] This compound exhibits the unprecedented property of ferromagnetic exchange within the Kagomé layer. Magnetic susceptibility[20] and neutron diffraction[21] studies reveal characteristics of a metamagnet, arising from the antiferromagnetic coupling of neighboring ferromagnetic layers below the critical temperature, T_c.

Interlayer coupling is a critical determinant for metamagnetism, which typically requires the confluence of low dimensionality imposed by a layered structure and anisotropic magnetic properties of the constituent magnetic centers.[22,23] The binary halides of divalent ions such as Fe^{2+}, Ni^{2+}, and Co^{2+} are archetypes for the investigation of the antiferromagnetic stacking of ferromagnetic sheets.[24−27] However, these are intractable materials from the standpoint of chemical modification, and the investigation of coupling between ferromagnetic layers has necessarily relied on using a scaffold such as graphite to control the separation between islands of metal dihalide multilayers.[28−31] Alternatively, the spacing of the layered hydroxides of M^{2+} ions can be reproducibly controlled at a molecular level by the intercalation of organic guest molecules.[32] Variation of the interlayer spacing of these hybrid organic−inorganic materials gives rise to a wide range of magnetic behavior, which includes metamagnetism. The challenges in obtaining single crystals of organic−inorganic hybrid materials for structural analysis, however, make it difficult to develop precise magneto-structural correlations for these materials.

To this end, the recent availability of the structurally characterized and homologous series of V^{3+} jarosites, $AV_3(OH)_6(SO_4)_2$ with $A = Na^+$, K^+, Rb^+, Tl^+, and NH_4^+,[13] provides a heretofore unavailable opportunity to systematically investigate the magnetism of a jarosite composed of ferromagnetic Kagomé layers. Single-crystal X-ray analysis of the $AV_3(OH)_6(SO_4)_2$ series reveals an isostructural intralayer; only the spacing between the layers is varied by A^+ substitution. The ability to precisely alter the interlayer spacing while preserving the intralayer structure, and consequently ferromagnetic coupling, allows us to examine how the antiferromagnetic coupling of ferromagnetic Kagomé layers depends on their separation. We now report the results of this inquiry and attendant magnetic studies of these novel layered materials.

Experimental Section

The $AV_3(OH)_6(SO_4)_2$ ($A = Na^+$, K^+, Rb^+, Tl^+, and NH_4^+) jarosite samples used in this study were prepared by reducing $VOCl_2$ with dimethylsulfite in acidic solutions containing the A^+ ion. The detailed hydrothermal conditions in which these oxidation−reduction reactions were carried out and the chemical analysis data for the materials used in this study are reported in the accompanying paper.[13] In all cases, stoichiometric materials are obtained. The magnetically dilute jarosite, $KGa_{2.96}V_{0.04}(OH)_6(SO_4)_2$, was prepared as follows: 523 mg of K_2SO_4 (3.0 mmol) and 0.33 mL of H_2SO_4 (6.0 mmol) were dissolved in 10 mL of distilled water and transferred into the Teflon liner of a 23-mL Parr pressure vessel. To the solution, 120 mg of Ga metal (1.72 mmol) and 11 mg of VCl_3 (0.070 mmol) were added. The vessel was enclosed and placed in an oven at 205 °C for 4 d. The vessel was subsequently cooled at 0.6 °C/min to afford an off-white suspension, which was filtered, washed with distilled water, and dried. Anal. Calcd for $H_6KGa_{2.96}V_{0.040}O_{14}S_2$: K 7.22 Ga 38.10, V 0.38, S 11.84, H 1.11. Found: K 6.56, Ga 38.60 V 0.68, S 12.25, H 1.20.

Magnetic susceptibilities were determined on powdered specimens contained in gelatin capsules using a SQUID susceptometer (Quantum Design MPMSR2 Susceptometer) over a 2−300 K temperature range and at field strengths varying from −50 to +50 kOe. These data were corrected for diamagnetic contributions of the sample holder and sample (χ_{core}), and for temperature-independent paramagnetism (χ_{TIP}). The values of χ_{core} and χ_{TIP} were determined by using a modified form of the Curie−Weiss law,

$$\chi_M^{-1} = \frac{T - \Theta_{CW}}{C + \chi_{const}(T - \Theta_{CW})} \quad (1)$$

where χ_M is the molar susceptibility, C is the Curie constant, Θ_{CW} is the Weiss constant, and χ_{const} is the fitting parameter that accounts for χ_{core} and χ_{TIP}. The presence of χ_{TIP} was detected experimentally by measuring the temperature dependence of the molar susceptibility of a 12-mg compressed pellet of $NaV_3(OH)_6(SO_4)_2$ over 300−500 K at various field strengths. We note that χ_{const} is field dependent, exhibiting a power law dependence of approximately $H^{-1/2}$. The origin of this effect is ascribed to a background signal, which is prominent for measurements conducted on specimens that produce weak signals (low mass and paramagnetic response at high temperature). The fitting procedure described by eq 1 accounts for the dependence of χ_{const} on

(13) Grohol, D.; Nocera, D. G. *J. Am. Chem. Soc.* **2002**, *124*, 2640−2646.
(14) Inami, T.; Nishiyama, M.; Maegawa, S.; Oka, Y. *Phys. Rev. B* **2000**, *61*, 12181−12186.
(15) Frunzke, J.; Hansen, T.; Harrison, A.; Lord, J. S.; Oakley, G. S.; Visser, D.; Wills, A. S. *J. Mater. Chem.* **2001**, *11*, 170-185.
(16) Earle, S. A.; Ramirez, A. P.; Cava, R. J. *Physica B* **1999**, *262*, 199−204.
(17) Harrison, A.; Wills, A. S.; Ritter, C. *Physica B* **1998**, *241−243*, 722−723.
(18) Lee, S.-H.; Broholm, C.; Collins, M. F.; Heller, L.; Ramirez, A. P.; Kloc, Ch.; Bucher, E.; Erwin, R. W.; Lacevic, N. *Phys. Rev. B* **1997**, *56*, 8091−8097.
(19) Keren, A.; Kojima, K.; Le, L. P.; Luke, G. M.; Wu, W. D.; Uemura, Y. J.; Takano, M.; Dabkowska, H.; Gingras, M. J. P. *Phys. Rev. B* **1996**, *53*, 6451−6454.
(20) Grohol, D.; Papoutsakis, D.; Nocera, D. G. *Angew. Chem., Int. Ed.* **2001**, *40*, 1519−1521.
(21) The magnetic structure of $NaV_3(OD)_6(SO_4)_2$ has been determined by neutron diffraction (Grohol, D.; Huang, Q. Z.; Lee, Y. S.; Toby, B. H.; Lynn, J. W.; Nocera, D. G., manuscript in preparation). A doubling of the magnetic unit cell is consistent with interlayer antiferromagnetic coupling of ferromagnetic Kagomé layers. Analysis of the neutron data leads to a model in which the magnetic moments lie within the plane of the Kagomé layer. These results are consistent with a recently published neutron diffraction study of $(H_3O)V_3(OH)_6(SO_4)_2$ (Wills, A. W. *Phys. Rev. B* **2001**, *63*, 064430/1−13).
(22) Stryjewski, E.; Giordano, N. *Adv. Phys.* **1977**, *26*, 487−650.
(23) Kurmoo, M. *Philos. Trans. R. Soc. London, Ser. A* **1999**, *357*, 3041−3061.
(24) Katori, H. A.; Katsumata, K.; Katori, M. *Phys. Rev. B* **1996**, *54*, R9620−R9623.
(25) Day, P. *Acc. Chem. Res.* **1988**, *21*, 250−254.
(26) Birgeneau, R. J.; Yelon, W. B.; Cohen, E.; Makovsky, J. *Phys. Rev. B* **1972**, *5*, 2607-2615.
(27) Lines, M. E. *Phys. Rev.* **1963**, *131*, 546−555.
(28) Elahy, M.; Dresselhaus, G. *Phys. Rev. B* **1984**, *30*, 7225−7235.
(29) Szeto, K. Y.; Chen, S. T.; Dresselhaus, G. *Phys. Rev. B* **1985**, *32*, 4628−4638.
(30) Szeto, K. Y.; Chen, S. T.; Dresselhaus, G. *Phys. Rev. B* **1986**, *33*, 3453−3459.
(31) Dresselhaus, G.; Dreselhaus, M. S.; Nicholls, J. T. *Springer Proc. Phys.* **1988**, *27*, 146−157 and references therein.
(32) Awaga, K.; Coronado, E.; Drillon, M. *Mater. Res. Soc. Bull.* **2000**, *25*, 52−57.

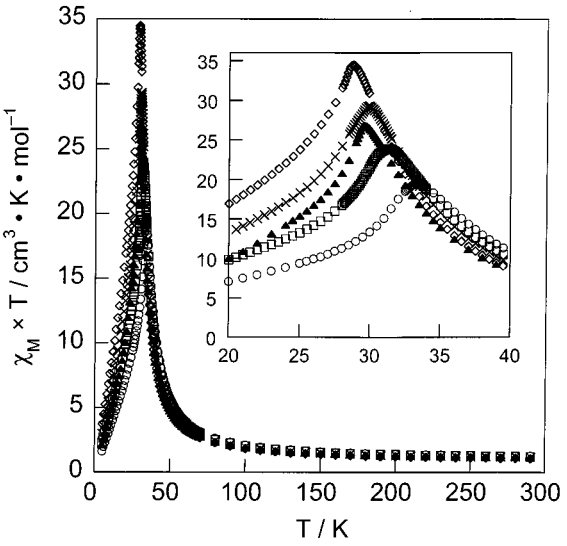

Figure 1. Temperature dependence of χ_M (per mole of vanadium) $\times$ T for $AV_3(OH)_6(SO_4)_2$, A = Na^+ (○), K^+ (□), Rb^+ (×), NH_4^+ (▲), and Tl^+ (◇). The inset highlights the shift of T_c along the series.

H and yields Curie and Weiss constants that are remarkably consistent for the different jarosite compounds.

Single-crystal magnetism studies of $NaV_3(OH)_6(SO_4)_2$ were performed on hexagonal plates with approximate dimensions of 0.1 mm × 0.1 mm × 0.02 mm. The hexagonal face of the crystal, which was not indexed on a diffractometer, was identified with the use of an optical microscope, and it was aligned (±10°) along the applied field direction. The perpendicular orientation (to give $M_\perp$ and $\chi_\perp$) assumes that the hexagonal crystal face coincides with the Kagomé layers. The crystal was then rotated by 90° to obtain magnetic susceptibility measurements in the parallel orientation ($M_{//}$ and $\chi_{//}$). The mass of the crystal was not accurately determined owing to its small size, which was also responsible for weak signals possessing appreciable background contributions. The background signal was dissimilar for crystal orientations parallel and orthogonal to the applied field. Data obtained for the two crystal orientations were therefore normalized to each other in the high-temperature regime.

Results

The magnetism of the V^{3+} jarosites has been investigated by monitoring the temperature and field dependence of the dc magnetic susceptibility. Figure 1 presents the temperature dependence of $\chi_M \times T$ per mol of V^{3+} ions at applied fields of 0.5 kOe. All samples exhibit the same magnetic kind of behavior, which is consistent with our preliminary observation of metamagnetism for $NaV_3(OH)_6(SO_4)_2$.[20,21] At high temperatures, $\chi_M \times T$ is constant and μ_{eff} values are 3.02 to 3.16, which are slightly higher than the spin-only $S = 1$ value of 2.83 μ_B. Inflated values of μ_{eff} for compounds possessing V^{3+} pairwise interactions can arise from the presence of ferromagnetic exchange[33−37] and/or the presence of temperature-independent diamagnetic contributions,[38] which are expected to arise from the appropriate orbital mixing within the d-manifold of a d^2 metal ion.[39−41] With the intent of distinguishing between these two potential contributions to μ_{eff}, the susceptibility was measured at high temperatures. The variance of χ_M^{-1} with T = 300−500 K and with field strengths ranging from 0.5 to 13 kOe is displayed in Figure 2a for $NaV_3(OH)_6(SO_4)_2$. The concave bend in the curves as temperature is increased suggests the presence of temperature independent paramagnetism (TIP), which will affect the Weiss constant and result in exaggerated values of μ_{eff}.[40] Moreover, the temperature independence of μ_{eff} up to 500 K suggests that ferromagnetic contributions to μ_{eff} are not prevalent at room temperature. Susceptibility data were corrected for TIP and other temperature independent contributions by using eq 1 to obtain χ_{const}, which was applied to the raw susceptibility of Figure 2a; Figure 2b replots the corrected χ_M^{-1} data. As should be the case for the paramagnetic regime, Curie−Weiss plots are linear and coincident over the 300−500 K range. Repeated measurements on the same specimens under different experimental conditions or on different samples of the same compound display remarkable consistency in the Curie and Weiss constants extracted from this fitting procedure.

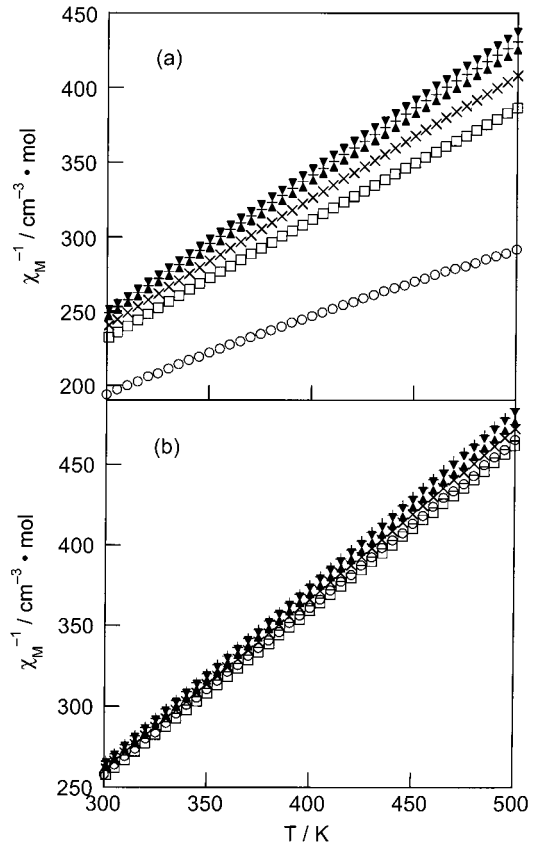

Figure 2. (a) Plot of χ_M^{-1} (per mole of vanadium) vs T of the raw data of $NaV_3(OH)_6(SO_4)_2$ at field strengths 0.5 (○), 3 (□), 5 (×), 8 (▲), 10 (+), and 13 (▼) kOe. (b) The same data using eq 1 to correct for χ_{TIP} and χ_{core} contributions.

Intralayer ferromagnetic coupling among neighboring V^{3+} centers is indicated by the upturn in $\chi_M \times T$ with decreasing T. Attendant to this upturn is the increase in μ_{eff} ranging from 20 to 30 μ_B at temperatures approaching the critical transition

(33) Weihe, H.; Güdel, H. U. *J. Am. Chem. Soc.* **1998**, *120*, 2870−2879.
(34) Brand, S. G.; Edelstein, N.; Hawkins, C. J.; Shalimoff, G.; Snow, M. R.; Tiekink, E. R. T. *Inorg. Chem.* **1990**, *29*, 434−438.
(35) Knopp, P.; Wieghardt, K.; Nuber, B.; Weiss, J.; Sheldrick, W. *Inorg. Chem.* **1990**, *29*, 363−371.
(36) Knopp, P.; Wieghardt, K. *Inorg. Chem.* **1991**, *30*, 4061−4066.
(37) Carrano, C. J.; Verastgue, R.; Bond, M. R. *Inorg. Chem.* **1993**, *32*, 3589−3590.
(38) Mahajan, A. V.; Johnston, D. C.; Torgeson, D. R.; Borsa, F. *Phys. Rev. B* **1992**, *46*, 10966−10972.
(39) Figgis, B. N. *Introduction to Ligand Fields*; Interscience: New York, 1966.
(40) Mabbs, F. E.; Machin, D. J. *Magnetism and Transition Metal Complexes*; Chapman and Hall: London, 1973.
(41) Carlin, R. L.; O'Connor, C. J.; Bhatia, S. N. *Inorg. Chem.* **1976**, *15*, 985−986.

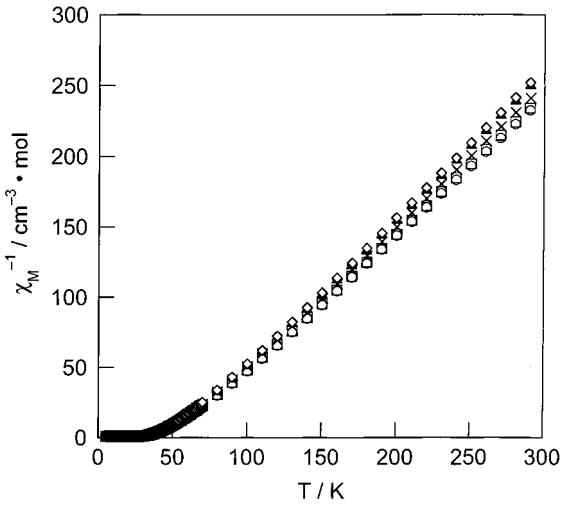

Figure 3. Plot of χ_M^{-1} (per mole of vanadium) vs T of $AV_3(OH)_6(SO_4)_2$, for A = Na^+ (○), K^+ (□), Rb^+ (×), NH_4^+ (▲), and Tl^+ (◇).

Table 1. Magnetic Parameters of $AV_3(OH)_6(SO_4)$ Jarosites

A^+	C[a]	Θ_{CW}/K[a]	T_c/K[b]
Na^+	1.01(1)	+54	33.3
K^+	1.00(1)	+54	31.0
Rb^+	0.99(1)	+52	29.8
NH_4+	0.95(1)	+53	29.5
Tl^+	0.94(1)	+53	28.5

[a] Determined from fits of the Curie−Weiss law in the 150−300 K temperature regime on data recorded at an external field of 5 kOe. [b] Determined from data recorded with an external field of 0.5 kOe.

temperature (T_c). Figure 3 shows the $\chi_M^{-1}(T)$ plots for the five samples. Extrapolation of the linear part of the Curie−Weiss plots to low temperatures yields large and positive intercepts. Nearly identical Curie and Weiss constants (Table 1) of $C \approx 1$ and $\Theta_{CW} = +53(1)$ K are obtained on all samples, regardless of the nature of the A^+ ion and the method of sample preparation.[13] This result emphasizes the advantage of our new synthetic methods over those used so far to afford pure and stoichiometric jarosites. The onset of 3-D antiferromagnetic ordering, originating from interlayer coupling, is observed below ~30 K as indicated by the presence of a sharp maximum in the $\chi_M \times T$ plot (Figure 1, inset) and the correspondent approach of μ_{eff} toward zero at low T. The critical temperatures listed in Table 1 increase monotonically from 28.5(1) K to 33.3(1) K along the series $Tl^+ < Rb^+ \approx NH_4^+ < K^+ < Na^+$.

The antiferromagnetic interlayer coupling is overcome by the application of an external field. Figure 4 displays the χ_M versus T plots for $NaV_3(OH)_6(SO_4)_2$ at field strengths of 0.5, 5, and 10 kOe; all other members of the V^{3+} jarosite series exhibit similar behavior. The sharp maximum at 33.3 K, observed for an external field of 0.5 kOe, is replaced by a broader peak centered at ~30.3 K when the external field of 5 kOe is applied. At applied fields ≥ 10 kOe, the maximum is completely suppressed and the susceptibility is observed to asymptotically approach a saturation value.[42] The critical field for this transition was estimated from a detailed examination of the field dependence of the magnetization shown in Figure 5. The maximum in the magnetization curve at 1.5 kOe attenuates slowly as field strengths are increased to ~6 kOe, after which it is eradicated. In the absence of quantitative single-crystal measurements, this

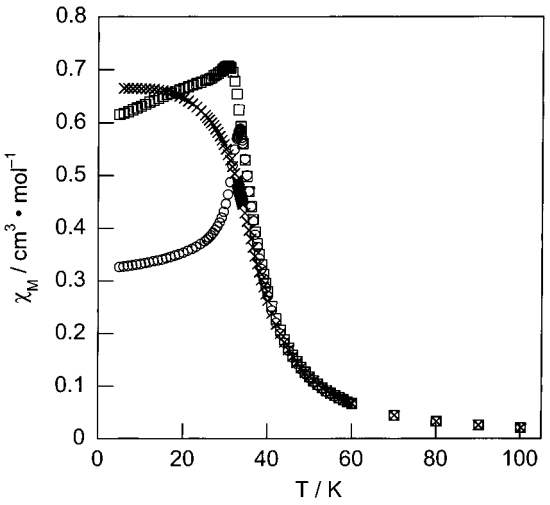

Figure 4. χ_M (per mole of vanadium) vs T plot of $NaV_3(OH)_6(SO_4)_2$ under external fields of H = 0.5 (○), 5 (□), and 10 (×) kOe. Data for the jarosites with $A^+ = K^+$, Rb^+, NH_4^+, and Tl^+ are similar.

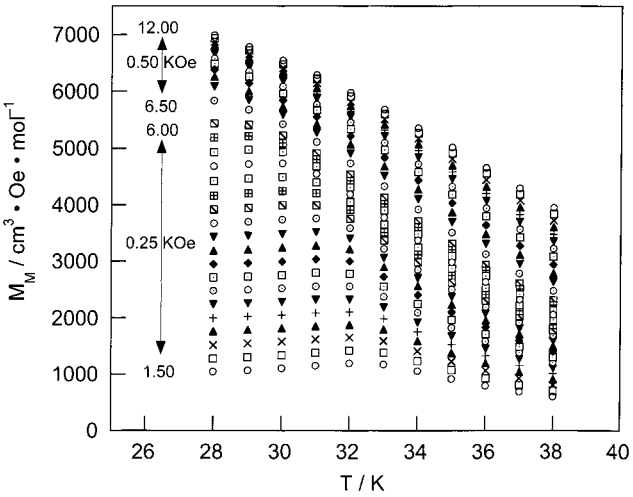

Figure 5. Temperature dependence of the molar magnetization (per mole of vanadium) in the 28−38 K temperature range at various applied field strengths (1.50−6.00 kOe with field increments of 0.25 kOe and 6.50−12.00 kOe with field increments of 0.50 kOe).

value of 6 kOe provides the best estimate of the field required to induce the antiferromagnetic to paramagnetic transition.

Metamagnetism of the $AV_3(OH)_6(SO_4)_2$ compounds is also apparent from the field-dependent behavior of magnetization. Figure 6 shows these data for $NaV_3(OH)_6(SO_4)_2$ samples cooled to 5 K. The magnetization curve exhibits the typical sigmoidal behavior expected for a metamagnet,[32] reaching saturation values that increased from 1.6 to the expected 2 $N\mu_B$ at $H > 10$ kOe. This variance in the saturation magnetization with field strength has been observed by Starr and Bitter[43] for the layered transition metal dihalides that display strong ferromagnetic coupling. These authors ascribe the field-dependent effect to preferential packing arrangements of platelets within the sample holder of individual

(42) At low fields, the magnetization, M, varies linearly with the field H, and M/H therefore represents the magnetic susceptibility of the material. At higher field strengths, however, and especially for materials with strong ferromagnetic interactions, magnetization depends nonlinearly on field strength, and consequently M/H does not represent the actual susceptibility. For this reason, the plots of M/H vs T at low temperatures show different shapes for different values of H. Further reference to this issue can be found in: DeFotis, G. C.; McGhee, E. M.; Bernal, I.; Losee, D. B. *J. Appl. Phys.* **1987**, *61*, 3298−3300.

(43) Starr, C.; Bitter, F.; Kaufmann, A. R. *Phys. Rev.* **1940**, *58*, 977−983.

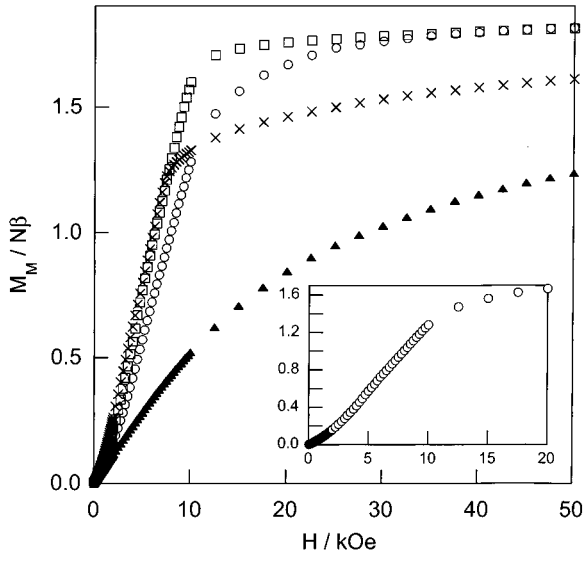

Figure 6. Magnetization (per mole of vanadium) vs applied field strength for $NaV_3(OH)_6(SO_4)_2$ at $T = 2$ (○), 5 (□), 25 (×), and 40 K (▲). The inset shows the 2 K data expanded over an abbreviated low field range.

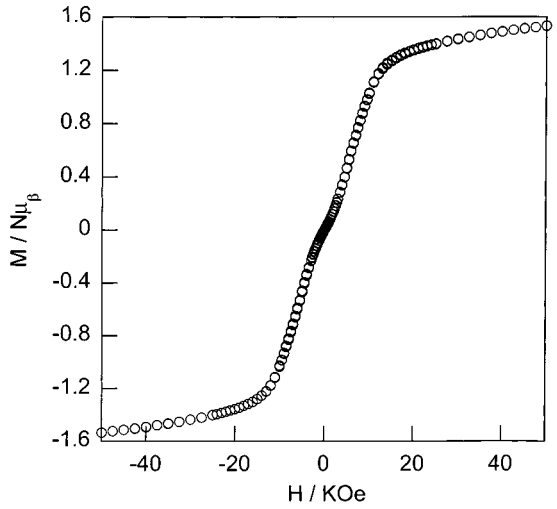

Figure 7. Magnetization (per mole of vanadium) as a function of applied field of $NaV_3(OH)_6(SO_4)_2$ at 5.0 K (○). Data for jarosites with $A^+ = K^+$, Rb^+, NH_4^+, and Tl^+ are similar.

crystallites to produce sample anisotropy. The application of corrections for demagnetizing fields is difficult because it is not certain if the specimen is behaving as a single material or if each crystal demagnetizes itself. With increasing temperature, the sigmoidal nature of the curve slowly fades, completely disappearing for temperatures above T_c. As highlighted in Figure 7, no hysteresis effect in the magnetization curve is observed.

Single-ion anisotropy, a common element of layered metamagnetism,[22] arises from the placement of a d^2 ion in the tetragonal crystal field of jarosite. We sought to assess the magnitude of this anisotropy by measuring the zero-field splitting (D) of a diamagnetic host jarosite, $AGa_3(OH)_6(SO_4)_2$, doped with magnetically dilute V(III) spin carriers. At the prepared stoichiometries of $KGa_{2.96}V_{0.04}(OH)_6(SO_4)_2$, short-range interactions among the V^{3+} ions are precluded, and the magnetic properties of the sample is expected to be consistent with the paramagnetic behavior of the ion in a D_{4h} environment. Figure 8a displays the temperature dependence of $\chi_M \times T$ over the

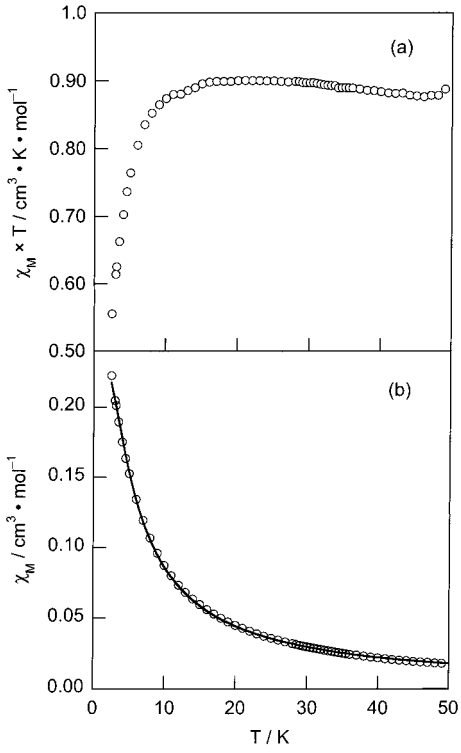

Figure 8. (a) Temperature dependence of χ_M (per mole of vanadium) × T for $KGa_{2.96}V_{0.04}(OH)_6(SO_4)_2$ (○). (b) Temperature dependence of the susceptibility χ_M (per mole of vanadium) of $KGa_{2.96}V_{0.04}(OH)_6(SO_4)_2$ (○). The solid line represents the best fit obtained by using eqs 3−5.

5−50 K temperature range for $KGa_{2.96}V_{0.04}(OH)_6(SO_4)_2$. The constant value of $\chi_M \times T$ at high temperatures corresponds to the expected spin-only moment for a V^{3+} paramagnetic ion. Below 10 K, the deviation of the $\chi_M \times T$ curve from linearity and its sharp decrease toward zero is ascribed to the zero-field splitting of the $^3A_2$ ground-state term. In an axial field, the $^3A_2$ ground state is described by the usual spin Hamiltonian for $S = 1$,[44]

$$\mathbf{H} = g_{\parallel}\mu_B H S_z + g_{\perp}\mu_B[H_x S_x + H_y S_y] + D[S_z^2 - {}^1/_3 S(S+1)] \quad (2)$$

and the following equations are derived for the molar susceptibility:

$$\chi_{\parallel} = \frac{2Ng_{\parallel}^2\mu_B^2}{kT}\exp(-D/kT)[1 + 2\exp(-D/kT)]^{-1} \quad (3)$$

$$\chi_{\perp} = \frac{2Ng_{\perp}^2\mu_B^2}{D}[1 - \exp(-D/kT)][1 + 2\exp(-D/kT)]^{-1} \quad (4)$$

$$\bar{\chi} = {}^1/_3(\chi_{\parallel} + 2\chi_{\perp}) \quad (5)$$

Figure 8b displays the fit of χ_M versus T obtained by using eqs 3−5. A value of $D = +7.5$ K (5.2 cm^{-1}) is obtained for $g_{\parallel} = 1.95$ and $g_{\perp} = 1.87$, which were taken from high-field multifrequency EPR measurements of $[V(OH_2)_6]^{3+}$ doped into a $CsGa(SO_4)_2 \cdot 12H_2O$ matrix.[45] The use of g-values deduced from single-crystal susceptibility measurements of other V^{3+}

(44) Kahn, O. *Molecular Magnetism*; VCH: Weinheim, 1993.
(45) Tregenna-Piggott, P. L. W.; Weihe, H.; Bendix, J.; Barra, A.-L.; Güdel, H.-U. *Inorg. Chem.* **1999**, *38*, 5928−5929.

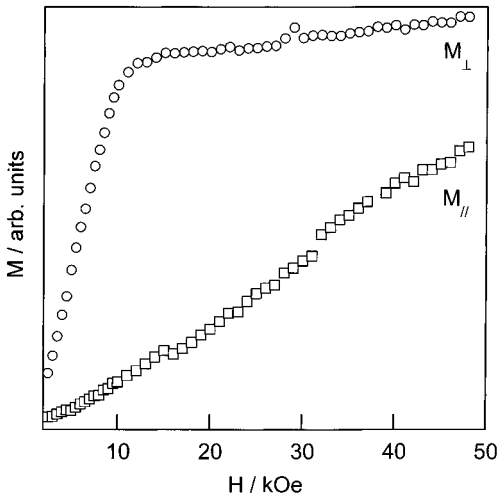

Figure 9. Magnetization vs H plot of a $NaV_3(OH)_6(SO_4)_2$ single crystal with an external field applied orthogonal (□, $M_{||}$) and parallel (○, $M_\perp$) to the Kagomé planes.

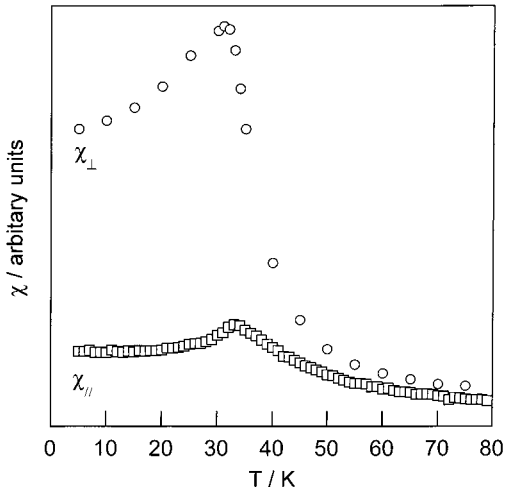

Figure 10. Susceptibility vs T plot of a $NaV_3(OH)_6(SO_4)_2$ single crystal with an external field applied orthogonal (□, $\chi_{||}$) and parallel (○, $\chi_\perp$) to the Kagomé plane.

compounds ($g_{||} = 1.93(2)$, $g_\perp = 1.74(2)$[46−49]) yielded similar D values. The D obtained from our fit of the data in Figure 8b is in excellent agreement with those reported for V^{3+} residing in other tetragonally distorted oxygen environments.[46−50]

Quantitative single-crystal measurements of the $AV_3(OH)_6(SO_4)_2$ series were attempted but these experiments were hampered by the small sizes of crystals, which typically possessed edge dimensions of ∼0.1 mm. Signals were weak and significantly influenced by background contributions. Moreover, the small crystal size prevented the unambiguous determination of crystal mass and orientation with respect to the applied field. Figure 9, which displays the field dependence behavior of the magnetization in the two orientations, is therefore of only qualitative value. $M_{||}$ increases linearly with field strength but does not saturate at applied fields approaching 50 kOe. Conversely, $M_\perp$ abruptly increases and attains a limiting value above 10 kOe. This magnetic anisotropy is also reflected in the temperature dependence of the susceptibility measured at field strengths of 3 kOe (Figure 10). Although $\chi_{||}$ and $\chi_\perp$ both display a maximum at T_c, $\chi_\perp$ increases much faster upon cooling below 50 K, whereas the value of $\chi_{||}$ remains roughly constant over the temperature range studied. The maximum ratio between the susceptibilities in the two orientations is between 4 and 5, consistent with the substantial single-ion anisotropy of the system.[50]

Discussion

The metamagnetic properties of the V^{3+} jarosites arise from the two competing interactions that were first identified by Landau[51]—ferromagnetic alignment of magnetic moments within a layer accompanied by a weaker antiferromagnetic coupling between neighboring layers. The intralayer ferromagnetic interactions are dominant at temperatures above ∼30 K, below which interlayer antiferromagnetic coupling becomes manifest to the overall magnetic properties of V^{3+} jarosite. Owing to its greater strength, the ferromagnetic ordering within the layer provides the impetus for the antiferromagnetic transition. Thus a discussion of the intralayer ferromagnetic ordering is the logical starting point for the interpretation of the magnetic properties of $AV_3(OH)_6(SO_4)_2$.

The large positive values of the Weiss constants of the $AV_3(OH)_6(SO_4)_2$ compounds reveal strong ferromagnetic interactions between adjacent V^{3+} sites. This observation is unusual for molecular or layered compounds of vanadium. Typically, antiferromagnetic ordering results from the interaction of spins along superexchange pathways comprising vanadium subunits linked by oxo or hydroxo bridging ligands. Most of these compounds possess d^1 or mixed-valence d^0/d^1 vanadium centers in a square pyramidal coordination geometry.[52−56] When ferromagnetic exchange is observed, the interaction is extremely weak with Weiss constants near 0 K.[57−59] For the d^2 electron count, short-range pairwise interactions between the V^{3+} centers of various binuclear compounds have been inferred from magnetic susceptibility data (although these observations require consideration of TIP).[33] In extended layered materials, ferromagnetic ordering among V^{3+} ions occurs as weak secondary interactions[60−63] arising from unquenched orbital momentum or from the canting of strongly aligned antiferromagnetic moments. In contrast, the strong intralayer ferromagnetism of

(46) Tregenna-Piggott, P. L. W.; Best, S. P.; Güdel, H.-U.; Weihe, H.; Wilson, C. C. *J. Solid State Chem.* **1999**, *145*, 460−470.
(47) Gregson, A. K.; Doddrell, D. M.; Healy, P. C. *Inorg. Chem.* **1978**, *15*, 1216−1219.
(48) Smit, J. J.; De Jongh, L. J.; De Klerk, D.; Carlin, R. L.; O'Connor, C. J. *Physica B* **1977**, *86−88*, 1147−1148.
(49) Mahalingam, L. M.; Friedberg, S. A. *Physica B* **1977**, *86−88*, 1149−1150.
(50) Carlin, R. L. *Magnetochemistry*; Springer-Verlag: Berlin, 1986.
(51) Landau, L. *Physik. Z. Sowjetunion* **1933**, *4*, 675.
(52) Clearfield, A. *Prog. Inorg. Chem.* **1998**, *47*, 371−510.
(53) Le Bideau, J.; Papoutsakis, D.; Jackson, J. E.; Nocera, D. G. *J. Am. Chem. Soc.* **1997**, *119*, 1313−1316.
(54) Amorós, P.; Marcos, M. D.; Beltrán-Porter, A.; Beltrán-Porter, D. *Curr. Opin. Solid State Mater. Sci.* **1999**, *4*, 123−131.
(55) Beltrán-Porter, D.; Beltrán-Porter, A.; Amorós, P.; Ibáñez, R.; Martinez, E.; Le Bail, A.; Ferey, G.; Villeneuve, G. *Eur. J. Solid State Inorg. Chem.* **1991**, *28*, 131−161.
(56) Beltrán-Porter, D.; Amorós, P.; Ibáñez, R.; Le Bail, A.; Ferey, G.; Villeneuve, G. *Solid State Ionics* **1989**, *32*, 57−69.
(57) Villeneuve, G.; Lezama, L.; Rojo, T. *Mol. Cryst. Liq. Cryst.* **1989**, *176*, 495−506.
(58) Papoutsakis, D.; Jackson, J. E.; Nocera, D. G. *Inorg. Chem.* **1996**, *35*, 800−801.
(59) Yamase, T.; Makino, T. H. *J. Chem. Soc., Dalton Trans.* **2000**, *7*, 1143−1150.
(60) Nguyen, H. C.; Goodenough, J. B. *Phys. Rev B* **1995**, *52*, 324−334.
(61) Goodenough, J. B.; Nguyen, H. C. *C. R. Acad. Sci.* **1994**, *319*, 1285−1291.
(62) Ren, Y.; Palstra, T. T. M.; Khomskii, D. I.; Pellegrin, E.; Nugroho, A. A.; Menovsky, A. A.; Sawatzky, G. A. *Nature* **1998**, *396*, 441−444.
(63) Kanke, Y. *Phys. Rev. B* **1999**, *60*, 3764−3776.

Table 2. Structural Comparison of Transition Metal Jarosites

	$AV_3(OH)_6(SO_4)_2$				$ACr_3(OH)_6(SO_4)_2$	$AFe_3(OH)_6(SO_4)_2$			
	Na^+ [a]	K^+ [a]	Rb^+ [a]	Tl^+ [a]	K^+ [b]	Na^+ [c]	K^+ [c]	Rb^+ [c]	ND_4^+ [d]
S−O(1)	1.461(8)	1.461(11)	1.458(11)	1.465(10)	1.428	1.462(7)	1.460(7)	1.452(10)	-
S−O(2)	1.476(5)	1.471(6)	1.478(7)	1.486(6)	1.488	1.483(4)	1.481(4)	1.481(5)	-
M−O(2)	2.054(4)	2.063(5)	2.064(6)	2.055(5)	1.979	2.061(4)	2.066(4)	2.070(5)	2.036(4)
M−O(3)	1.989(2)	1.991(2)	1.988(3)	1.983(2)	1.973	1.994(2)	1.987(2)	1.984(2)	1.9939(15)
M−M	3.643	3.637	3.640	3.642	3.619	3.671	3.652	3.657	3.6642(2)
A−O(2)	2.949(5)	2.975(6)	2.998(6)	3.002(6)	2.945	2.961(4)	2.971(4)	2.999(5)	-
A−O(3)	2.756(4)	2.851(5)	2.928(6)	2.943(5)	2.784	2.727(4)	2.826(4)	2.902(5)	-
O(2)−M−O(3)	92.53(14)	92.40(19)	92.0(2)	91.64(18)	-	91.84(13)	91.77(13)	91.04(17)	-
O(2)−M−O(3)	87.48(14)	87.60(19)	88.0(2)	88.36(18)	-	88.16(13)	88.23(13)	88.96(17)	-
O(3)−M−O(3)	90.9(3)	90.5(3)	91.0(4)	90.5(3)	-	91.8(3)	90.5(2)	90.1(3)	-
O(3)−M−O(3)	89.1(3)	89.5(3)	89.0(4)	89.5(3)	-	88.2(3)	89.5(2)	89.9(3)	-
M−O(3)−M	132.6	132.0	132.5	133.4	132.9	134.0	133.6	134.4	133.51
c axis	16.851(2)	17.399(2)	17.835(7)	17.919(2)	16.9544	16.605	17.185(2)	17.568(3)	17.3024(8)

[a] Single-crystal X-ray study conducted at 183 K (ref 13). [b] Neutron diffraction study conducted at 20 K in a sample containing ∼76(5)% of Cr^{3+} (ref 18). Bond distances and angles were determined by using the atomic coordinates given in ref 18. [c] Single-crystal X-ray study conducted at 183 K (ref 66). [d] Neutron diffraction study conducted at 1.5 K (ref 19).

$AV_3(OH)_6(SO_4)_2$ compounds is a primary interaction mediated by the pairwise coupling of V^{3+} spin carriers within the triangular Kagomé network.

The remarkable consistency of the measured Weiss constant across the $AV_3(OH)_6(SO_4)_2$ series of the five compounds suggests that substitution of the A^+ ion does not structurally perturb the $V^{III}_3(\mu\text{-}OH)_3$ triangles composing the Kagomé lattice. This contention is verified by the X-ray crystal structures of the $AV_3(OH)_6(SO_4)_2$ compounds for A = Na^+, K^+, Rb^+, and Tl^+.[13] Table 2 summarizes important bond distances and angles within the Kagomé layer. Little variation is observed in the metrics of the axially elongated octahedrons, which possesses nearly ideal D_{4h} symmetry as indicated by O−V−O angles of ∼90°. The axial vanadium-oxo bonds differ by less than 0.01 Å among the four structurally characterized materials (d_{avg}(V−O(2)) = 2.059(3) Å) and the variation in the equatorial hydroxyl bond length is even smaller (0.008 Å) d_{avg}(V−O(3)) = 1.988(2) Å).

Axial elongation of the vanadium octahedron lifts the degeneracy of the t_{2g} orbital set of an O_h crystal field. In the D_{4h} point group, a lower energy, half-filled, doubly degenerate e_g (d_{xz}, d_{yz}) orbital set and an empty, singly degenerate b_{2g} (d_{xy}) orbital is obtained.[64] The electronic ground state is an $^3A_2$ state, which splits to an E state and a lowest energy A_1 state.[50,65] The zero-field splitting, *D*, defines the energy separation between these two states. A positive *D* value for V^{3+} compounds establishes that the magnetic moment lies within the equatorial plane.[45,46] Such large single-ion anisotropy in the V^{3+} jarosites is expected to favor the preferential alignment of the magnetic moments within the Kagomé layers, which behave as the easy plane (as opposed to easy axis, which is more unlikely in view of the tetragonal symmetry of the system) of magnetization. The qualitative, single-crystal susceptibility measurements, as well as recent powder neutron diffraction data,[21] are consistent with this deduction. Facile saturation of the magnetization is observed for applied fields >10 kOe (at 5 K) when the crystal is oriented with the Kagomé layers parallel ($M_\perp$) to the external magnetic field. In this orientation, the intralayer moments are already ferromagnetically aligned and only the weak interlayer antiferromagnetic interaction needs to be overcome. In contrast, when the field is orthogonal to the Kagomé layers ($M_{||}$), the magnetic moments must be positioned along the hard axis. In this orientation, the single-ion anisotropy must be overcome in addition to the interlayer antiferromagnetic coupling. Consequently, as observed in Figure 9, the magnetization does not saturate, even with the application of strong external fields (50 kOe).

The intralayer ferromagnetism of $AV_3(OH)_6(SO_4)_2$ has no obvious structural basis. Table 2 lists metric parameters for Fe^{3+}, Cr^{3+}, and V^{3+} derivatives of jarosite. Single X-ray crystal data for seven derivatives (A = Na^+, K^+, Rb^+, Tl^+ for V^{3+} jarosites[13] and A = Na^+, K^+, Rb^+ for Fe^{3+} jarosite[66]) were collected at *T* = 183(2) K on the stoichiometrically pure samples afforded from our newly developed synthetic methods. Direct structural comparisons are therefore most reliable among these compounds. The structures of $Fe^{3+}(NH_4^+)$ and $Cr^{3+}(K^+)$ jarosites were determined from powder neutron diffraction analysis performed at much lower temperatures on samples possessing substantial vacancies at the A^+ and M^{3+} ion sites.[18,19] Their inclusion in a comparative structural study, therefore, is more tenuous. Notwithstanding, an important result emerges from Table 2. Namely, the intralayer framework of the Kagomé lattice of jarosite is structurally unaltered with d-electron count and with different A^+ ions. Excluding the two structurally disavowed systems, which only marginally display metrics outside those of their congeners, the equatorial M^{3+}−O(3) and axial M^{3+}−O(2) bond distances are almost constant across the series of compounds, differing by less than ∼0.01 and ∼0.02 Å, respectively. Similarly, the dimensions of the capping sulfate anion remain unperturbed across the series. The M^{3+}−O(3)−M^{3+} angle, which is considered to play a profound role in a possible superexchange pathway (vide infra), varies by only ∼2°. This structural integrity of the intralayer is quite remarkable when one considers that a change in the d-electron count from d^2 to d^3 and d^5 involves the population of predominantly metal π^*(d_{xy}) and σ^*(d_{z^2} and $d_{x^2-y^2}$) orbitals, respectively. We ascribe the structural insensitivity of the intralayer to the rigidity of the SO_4^{2-} capping group, which defines the dimension of the $M^{III}_3(\mu\text{-}OH)_3$ triangles. In view of this structural homology of the jarosites, their disparate magnetic properties likely arise from different stereoelectronic properties of the populated orbitals

(64) Webb, G. A. *Coord. Chem. Rev.* **1969**, *4*, 107−145.
(65) Figgis, B. N.; Lewis, J.; Mabbs, F. E. *J. Chem. Soc.* **1960**, 2480−2485.
(66) Grohol, D.; Papoutsakis, D.; Nocera, D. G. Submitted for publication.

of the M^{3+} center. The strong intralayer ferromagnetism of the V^{3+} jarosites originates from electrons residing in the (d_{xz},d_{yz}) orbital set. The sign of the exchange coupling changes for Cr^{3+} jarosite when an additional electron is added to the d_{xy} orbital. Placement of two more electrons in the d_{z^2} and $d_{x^2-y^2}$ orbitals of Fe^{3+} jarosite increases this antiferromagnetic exchange interaction within the Kagomé lattice by more than an order of magnitude.

Insight into the trend of the magnetic properties with d-electron count may be gleaned from an analysis of the orbital interactions of neighboring spin carriers and intervening ligand orbitals within $M^{III}_3(\mu\text{-OH})_3$ triangles of the Kagomé lattice. Pairwise orbital interactions were considered within the elementary $M^{III}_3(\mu\text{-OH})_3$ structural unit, which adopts a six-membered cyclohexane ring-like conformation with $O(3)-M^{3+}-O(3)$ angles of ~90° and $M^{3+}-O(3)-M^{3+}$ angles of ~135° (O(3) = equatorial hydroxyl oxygen). Scheme 1 presents the σ-orbital

Scheme 1

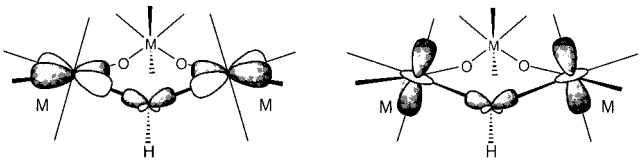

σ pathway (metal: $d_{x^2-y^2}$; oxygen: sp^2) σ pathway (metal: d_{z^2}; oxygen: sp^2)

interactions of the ring subunit in an edge-on orientation. For the d^5 case of $M^{3+} = Fe^{3+}$, the primary contribution to antiferromagnetism arises from the σ interaction comprising metal $d_{x^2-y^2}$ and d_{z^2} orbitals and the sp^2 hydroxyl orbitals of the $Fe^{3+}-O-Fe^{3+}$ bridge. Of these two orbitals, Goodenough-Kanamori rules[67−69] predict a primary and strong antiferromagnetic exchange interaction to proceed through the $d_{x^2-y^2}$ orbitals of a $M^{3+}-O-M^{3+}$ pathway with an angle exceeding 90°. This superexchange pathway is manifest to the magnetic properties of a variety of metal complexes bridged by oxygen ligands[44] and it has been previously suggested to be dominant in the intralayers of Fe^{3+} jarosite.[70] An additional antiferromagnetic exchange contribution is possible through the sulfate bridge but this superexchange contribution to the overall magnetism should be comparatively small owing to the greater number of bonds composing this path. Moreover, overlap between the d_{z^2} orbitals and the sp^2 orbitals of the bridging hydroxyl (right panel of Scheme 1) is expected to be small. For these reasons, the participation of the d_{z^2} orbitals in the overall exchange pathway should be insignificant. This contention could be tested with the preparation of Mn^{3+} jarosite, which will differ from its Cr^{3+} counterpart only by the population of d_{z^2} orbital. If the contribution of d_{z^2} to the superexchange pathway is negligible, then similar Weiss constants should be observed for the d^3 and d^4 jarosite systems.

In contrast to a d^5 Kagomé lattice, a description of the orbital interactions leading to the observed exchange coupling for the d^2 and d^3 systems within a frontier orbital framework is more cumbersome. The relevant orbital interactions are necessarily of π symmetry, involving sp^2 and p orbitals from the hydroxyl group and the (d_{xz},d_{yz}) orbital set of the d^2 ion and additionally the d_{xy} orbital of the d^3 ion. An intervening hydroxyl group between the metals of bi-[37,71−74] and trinuclear[36] centers can significantly influence exchange coupling when it is deprotonated. Consideration of how short range magnetic interactions are affected by the disposition of a protonated hydroxyl group between magnetic centers, however, has only recently been addressed by computational analysis,[75] which clearly shows that a rotation of hydroxyl from the M−O−M plane strongly influences the sign and magnitude of exchange coupling. In the case of Scheme 2, the orientation of the hydroxyl between the

Scheme 2

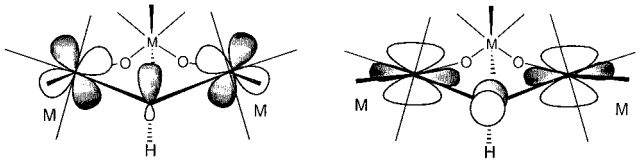

π pathway (metal: d_{xz}, d_{yz}; oxygen: sp^2) π pathway (metal: d_{xy}; oxygen: p)

two metal centers determines the extent to which the hydroxyl sp^2 and p orbitals mediate π-overlap and consequently magnetic exchange. Powder neutron diffraction studies of $NaV_3(OD)_6(SO_4)_2$ have allowed us to precisely determine that the O−D(H) bond is rotated ~18° from the V−O(3)−V plane and is nearly orthogonal to the O(3)−Na bond (H−O(3)−Na = 97.0°).[21] In this orientation, the sp^2 orbital of hydroxyl can preferentially interact with one d orbital of the (d_{xz},d_{yz}) pair (as illustrated in Scheme 2); the remaining d orbital of this pair interacts with the sp^2 orbital of the neighboring hydroxyl bridges (not shown). Inasmuch as a $d\pi-sp^2-d\pi$ interaction can give rise to both ferromagnetic and antiferromagnetic coupling,[44] the overall intralayer ferromagnetism of V^{3+} jarosite suggests the former exchange interaction to dominate for this π-symmetry pathway. In the case of Cr^{3+} jarosite, the $d\pi-sp^2-d\pi$ interaction is augmented by the additional π-bond formed between the hydroxyl p- and metal d_{xy} orbitals (see in the right panel of Scheme 2). The observation of a negative Weiss constant for Cr^{3+} jarosite implies that the antiferromagnetic term of the $p(OH)-d\pi$-interaction is dominant and able to overwhelm the ferromagnetic contribution of the $d\pi-sp^2-d\pi$ pathway.

The disposition of alternating metal atoms within a six-membered ring can potentially give rise to direct orbital exchange interactions. As established in Winstein's studies of homoaromaticity within the bicyclo[3.1.0]hex-3-yl cation,[76] alternating atoms within the six-membered ring of a cyclohexane conformer are poised to interact directly through-space. Within the $M_3(OH)_3$ cyclohexane subunits of V^{3+} and Cr^{3+} jarosites, direct exchange may occur from overlapping d_{xy}, d_{yz} ,and d_{xz} orbitals. An exchange pathway involving these orbitals has been computationally investigated within a face-shared bioctahedral framework.[77−80] For inter-metal separations of 2.6−3.2 Å,

(67) Goodenough, J. B. *J. Phys. Chem. Solids* **1958**, *6*, 287−297.
(68) Kanamori, J. *J. Phys. Chem. Solids* **1959**, *10*, 87−98.
(69) Ginsberg, A. P. *Inorg. Chim. Acta Rev.* **1971**, *5*, 45−68.
(70) Townsend, M. G.; Longworth, G.; Roudaut, E. *Phys. Rev. B* **1986**, *33*, 4919−4926.
(71) Hartman, J. A. R.; Rardin, R. L.; Chandhuri, P.; Paul, K.; Wieghardt, K.; Nuber, B.; Weiss, J.; Papaefthymiou, G. C.; Frankel, R. B.; Lippard, S. J. *J. Am. Chem. Soc.* **1987**, *109*, 7387−7396.
(72) Armstrong, W. H.; Lippard, S. J. *J. Am. Chem. Soc.* **1984**, *106*, 4632−4633.
(73) Armstrong, W. H.; Spool, A.; Papaefthymiou, G. C.; Frankel, R. B.; Lippard, S. J. *J. Am. Chem. Soc.* **1984**, *106*, 3653-3667.
(74) Kurtz, D. J., Jr. *Chem. Rev.* **1990**, *90*, 585−606.
(75) Ruiz, E.; Alemany, P.; Alvarez, S.; Cano, J. *J. Am. Chem. Soc.* **1997**, *119*, 1297−1303.
(76) Winstein, S. *Quart. Rev. Chem. Soc.* **1969**, *23*, 141−176.

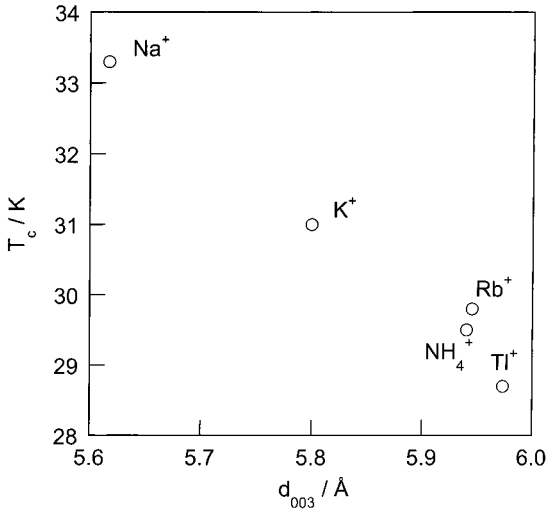

Figure 11. Plot of T_c against the interlayer space for the five $AV_3(OH)_6(SO_4)_2$ derivatives.

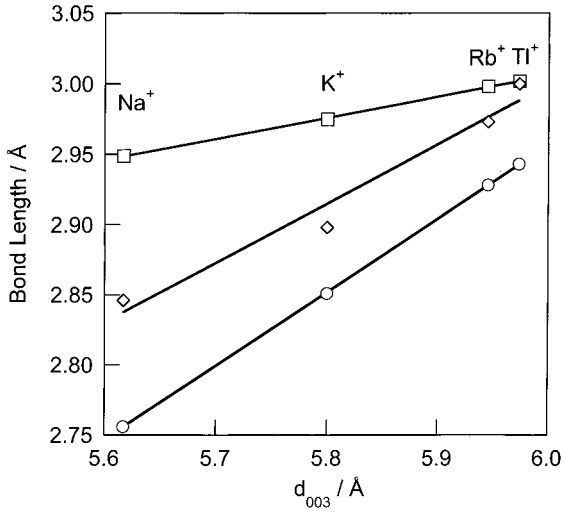

Figure 12. Plot of A−O(2) (□), A−O(3) (○) and O(3)−O(1) (◇) bond distances against the interlayer spacing for the four crystallographically characterized $AV_3(OH)_6(SO_4)_2$ derivatives.

through-space orbital interactions are observed to produce antiferromagnetic and ferromagnetic ground spin states, depending on orbital occupancy and metal−metal distance. The spin carrying metal atoms of the isostructural $M_3(OH)_3$ cyclohexane subunits are positioned ∼3.6 Å from each other. The longer inter-metal distances in the $M_3(OH)_3$ cyclohexane ring diminishes the significance of the through-space component, especially since the polyhedra of the metal ions do not share common edges or faces. This latter criterion has been identified as an important element for direct exchange between metal ions situated within octahedral or pseudo-octahedral coordination environments.[81]

In contradistinction to the antiferromagnetic properties of Fe^{3+} and Cr^{3+} jarosite intralayers, strong ferromagnetic exchange within V^{3+} jarosite layers provides a mechanism for interlayer antiferromagnetic exchange. Figure 11 shows that the interaction between neighboring layers decreases with increasing layer separation. The critical temperature scales linearly with interlayer spacing for the $AV_3(OH)_6(SO_4)_2$ systems. Communication between neighboring layers can be achieved either through dipole−dipole interactions or through superexchange pathways that either involve hydrogen bonds, the interlayer cations, or a combination of both. Superexchange through interlayer bond pathways, when present, is expected to carry the 3-D antiferromagnetic ordering between layers separated by small distances (<10 Å).[82] For the V^{3+} jarosites, spin sites in neighboring layers may connect along two distinct pathways. The M^{3+}−O(2,3)−A^+−O(2,3)−M^{3+} (O(3) = equatorial hydroxyl oxygen and O(2) = axial oxygen of sulfate) pathway involves connection through the interlayer A^+ cation; this four-bond pathway expands to a six-bond pathway when the alkali metal cation is replaced by the NH_4^+ ion. A second, more circuitous, pathway bypasses the alkali ion by involving the sulfate anion, M^{3+}−O(2)−S−O(1)···H−O(3)−M^{3+}. This six-bond pathway contains one hydrogen bond, which is defined structurally by the O(3)−O(1) distance. As hydrogen bonds are effective in mediating exchange in layered systems,[83] either of the two pathways are viable alternatives. As Figure 12 shows, however, their importance to the overall exchange pathway cannot be structurally distinguished as the d spacing of the V^{3+} jarosites scales linearly with the A−O(2,3) and O(1)−O(3) bond distances.

Conclusions

The vanadium jarosites display strong ferromagnetic interactions that are unprecedented in Kagomé layers. The intralayer coupling is invariant with the nature of the A^+ cation in the five compounds presented here. The single-ion anisotropy of the V^{3+} cation confines the exchange-coupled moments to lie within the Kagomé plane with sufficient coupling strengths to prevent saturation of the magnetization when an external field is applied orthogonal to the Kagomé plane. Weak interlayer antiferromagnetic coupling of the ferromagnetic Kagomé layers becomes dominant below ∼30 K, giving rise to overall 3-D metamagnetic behavior for the $AV_3(OH)_6(SO_4)_2$ jarosites. This interlayer exchange coupling may be overcome by the action of a sufficiently strong field, which is estimated to be ∼6 kOe. We have been able to unequivocally establish the magneto-structural correlation of decreasing antiferromagnetic coupling with increasing interlayer separation for the layered metamagnet because the bond angles and distances within the Kagomé lattice are not structurally perturbed by A^+ substitution.

More generally, the jarosites offer a unique framework in which to study magnetic exchange in the triangular lattice. Since magnetism responds to small structural changes in the local coordination environment of magnetic ions, specific stereoelectronic contributions to observed magnetic properties are difficult to isolate. As highlighted by the data of Table 2, the Kagomé lattice of jarosites circumvents this impediment by permitting electronic parameters such as d-electron count to be manipulated independently from structural perturbations. The properties of V^{3+} jarosite, together with those of its Cr^{3+} and

(77) Stranger, R.; McGrady, J. E.; Lovell, T. *Inorg. Chem.* **1998**, *37*, 6795−6806.
(78) McGrady, J. E.; Stranger, R.; Lovell, T. *Inorg. Chem.* **1998**, *37*, 3802−3808.
(79) McGrady, J. E.; Lovell, T.; Stranger, R. *Inorg. Chem.* **1997**, *36*, 3242−3247.
(80) Lovell, T.; McGrady, J. E.; Stranger, R.; Macgregor, S. A. *Inorg. Chem.* **1996**, *35*, 3079−3080.
(81) Goodenough, J. B. *Phys. Rev.* **1960**, *117*, 1442−1451.
(82) Drillon, M.; Panissod, P. *J. Magn. Magn. Mater.* **1998**, *188*, 93−99.
(83) Papoutsakis, D.; Kirby, J. P.; Jackson, J. E.; Nocera, D. G.; *Chem. Eur. J.* **1999** *5*, 1474−1480 and references therein.

Fe^{3+} congeners, allow us to correlate the sign and magnitude of exchange coupling within isostructural Kagomé layers to different orbital parentages engendered by the M^{3+} d-electron count. A frontier orbital analysis suggests that standard σ-orbital interactions are substantially augmented by π-orbital interactions, and it is these latter orbital pathways that are determinant to ferromagnetism within the Kagomé layers of jarosites. A more thorough understanding of the role of the π-interactions in mediating exchange coupling of jarosites calls for the preparation and study of materials with additional d-electron counts. These studies are currently underway.

Acknowledgment. We thank Dr. Young Lee for helpful discussions. Financial support for this work was provided by the National Science Foundation (DMR-9311597) and by a seed grant from the MIT Center for Materials Science and Engineering Research (DMR-9808941).

JA016833M